TEVATRON MAGNETIC MODELS
GEOMETRIC AND HYSTERETIC MULTIPOLES IN THE TEVATRON DIPOLE
Revision 2 – 04/05/2004

P. Bauer[1], J. Blowers, N. Gelfand, R.W. Hanft, D.J. Harding, M.J. Lamm,
G.L. Sabbi*, P. Schlabach, J.C. Tompkins, G. Velev

Fermilab, Technical and Beams Division
*LBNL, Accelerator and Fusion Research Division

Emmitance blow-up and beam loss are among the main limitations to ultimate luminosity in the Tevatron, currently in its run-II stage. It is well known that tunes and chromaticities are changing as the magnetic multipoles of the superconducting magnets decay during injection and snap-back during the ensuing start of the ramp. Fast changing tunes and chromaticities could contribute to the luminosity limitations. In the context of a renewed effort to improve the quantitative understanding of the decay and snapback characteristics of the superconducting magnets in the Tevatron, a series of magnetic measurements on spare Tevatron dipoles was started in the fall of 2002. In order to support the magnetic measurements, magnetic field models of the Tevatron dipole magnets were generated. The models were calibrated on the archival magnetic measurement data of all Tevatron dipoles built as well as on recent magnetic measurements. The magnetic model of the Tevatron dipole magnet presented here is therefore believed to be representative of the "average" Tevatron dipole magnet. This note was updated in November 2003 to include the results of z-scan measurements in a Tevatron dipole using a short rotating coil probe. These measurements were used to fine-tune the end-field model. The improved end-field model is presented. The second revision in April 2004 includes new calculations of the multipole hysteresis due to the superconductor magnetization.

---

[1] e-mail: pbauer@fnal.gov

TABLE OF CONTENTS

1)   Introduction

The Tevatron proton antiproton collider operates since 1983 and is currently in its collider run-II stage. Its lattice consists mainly of 774, 6 m long superconducting arc dipole magnets (or more exactly 772 full length dipoles and 2 half length dipoles in the C0 section) and 180 superconducting arc quadrupole magnets to accelerate and store proton and antiproton beams at 980 GeV energy. Figure 1 shows a cross sectional view of a Tevatron dipole magnet. The main features of this magnet are: a two-layer, wedge-less cosine-theta coil, a warm iron yoke, a compact multi-layer cryostat assembly around the stainless steel collars and four diagonal support bolts in the nine suspension stations along the magnet. Another noteworthy particularity of the Tevatron magnet is that it is a four-terminal magnet because its coils include the return bus as one of the outer layer mid-plane turns (first quadrant). The bus turn has a thick insulation to prevent breakdown at high voltage.

The following presents the results of a recent magnetic modeling effort, undertaken in the context of a resurgence of interest in the dynamic properties of the Tevatron main magnets related to the efforts to increase the luminosity of the Tevatron collider. Unlike traditional magnetic design studies, this particular modeling effort was conducted on an already mass-produced magnet. The results of the magnetic measurements performed during production have therefore been considered first.
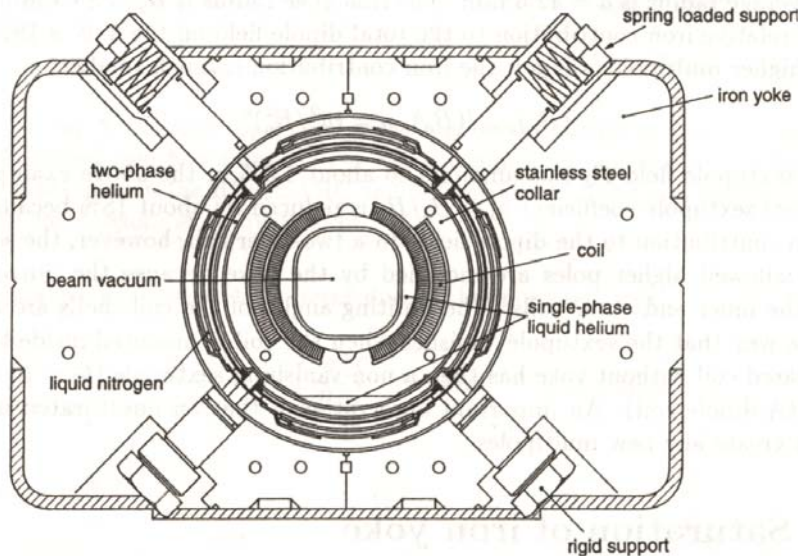

Figure 1: Tevatron dipole cross-section.

2)   Tevatron Dipole Harmonics Archive

The collected results of the magnetic measurements that were performed in the course of the Tevatron magnet production at Fermilab's Magnet Test Facility (MTF) have been reported at various conferences (e.g. [1]) and published in technical notes (e.g. [2]). Magnetic measurements were performed at different stages of the production of a

Tevatron magnet. Most important, however, were the magnetic measurements of the completed magnets in cold conditions, before and after "smart-bolting" (smart bolting refers to the use of smart bolts to minimize skew and normal quadrupoles by centering the coils within the yoke). The measurements were performed at MTF using 95" (2.413 m) long radial probes, placed in the ends and body of the magnet, therefore sampling the magnetic field over the entire length of the dipole. The integrated analog voltage (after bucking of the dipole signal) from the radial probe versus the probe angle data were Fourier analyzed to extract multipole data up to the 30-pole according to the standard multipole expansion (equation 1). The results were scaled with standard laws to the Tevatron reference radius of 1" (25.4 mm). The strength of the multipoles at the reference radius is given in units of 10^{-4} of the dipole strength. The measurements included not only the geometric multipoles (measured at high current) but also points along the hysteretic loop (at 600 A, 700 A, 2000 A and 4000 A). The number of points represents the minimum needed to reconstruct with sufficient precision the entire hysteretic loop. The magnet temperature during the measurements was typically 4.65 K.

$$B_y + iB_x = B_0 \sum_{n=0} \left(\frac{x+iy}{R_{ref}} \right)^n 10^{-4}(b_n + ia_n) \quad \left(multipole\, coeff.(a_n, b_n)\ in\ units\ of\ 10^{-4} B_0\, @R_{ref} \right)$$

(1)

Table 1 summarizes the magnetic multipoles (up to the 26-pole) in the body, ends and the body-end combined, averaged over all Tevatron dipoles currently in the ring as listed in the Tevatron multipole database [3]. The multipoles are quoted according to the US-convention (equ. 1). The normal sextupole is denoted b_2, the normal decapole b_4, etc.. To obtain the geometric multipoles from the measured hysteretic multipoles, the average of the multipole value at 2000 A over the up-and-down ramps was computed (only at 2000 A there is an up- and a down-ramp point). This particular procedure was chosen because the magnetic measurements were not taken on the fly (as it is done today), but the ramp was stopped during each measurement (to allow for a pre-wind of the measurement probe and the subsequent measurement during the un-wind). As we know today the measurements therefore include an unknown (and varying) amount of drift. By taking the multipole value lying between the up and down ramp, the geometric multipole can be derived exactly if the drift amplitudes during the up-and-down branches are identical. Note, however, that the drift at 2000 A is small (the total sextupole hysteresis width at that current is ~ 1.5 units and the possible drift can thus be estimated to be of the order of 0.1 units). Unfortunately an additional problem related to current overshoots on the down-ramp can occasionally perturb the symmetry of the hysteretic loop and therefore introduce some error into the result as obtained with the above procedure. The current overshoots were not corrected for in the data shown in Table 1.

The end and body multipoles listed in Table 1 represent the field quality of the average Tevatron dipole magnet in terms of a step-function profile. The constant body multipoles change to the constant (up-and downstream) end multipoles in a step. A typical b_2 step profile is shown in Figure 17 in section 4.3.). The combined data represent a weighted average of body- and end-fields (equ. 2). The weighting factor is the length integrated dipole signal, the so-called standard amplitude, for the body and the two end

measurements. The standard amplitude, in arbitrary units and at a given current of 1000 A, is typically 7000 in the body and 5700 in the end. Therefore the multiplier for the body field in the combination procedure is typically 7000/(7000+2·5700)=0.38. The multiplier for the end-field is 5700/(7000+2·5700) =0.31. The standard amplitudes are stored on a case-by-case basis in the data archive and therefore the weighting factors were calculated for each magnet. Ideally, the probe's positions in the body and end measurements were back-to-back, with neither gaps, nor overlaps. The ratios of the standard amplitude numbers tell to what extent that was actually the case. Often $B_{0,end}$ is assumed to be $B_{0,body}$ and L_{end} modified, such as to produce the required standard amplitude. This is the concept behind the so-called magnetic length, which will be discussed further in the following.

$$ b_n^{tot} = \frac{b_n^{body}L_{body}B_{0,body} + b_n^{u-end}L_{u-end}B_{0,u-end} + b_n^{d-end}L_{d-end}B_{0,d-end}}{L_{body}B_{0,body} + L_{u-end}B_{0,u-end} + L_{d-end}B_{0,d-end}} $$

(2)

   Figure 2 and Figure 3 show the geometric sextupole data for the body and ends of all 774 Tevatron dipoles. The plots show an initial production trend toward larger b_2, which was subsequently corrected. The Tevatron dipoles are characterized by a large negative sextupole in the ends because of their simple, compact end design. This will be discussed in further detail in section 4. The cross-section coil design was therefore chosen such as to produce a small positive sextupole, which compensates for the end sextupoles. Ideally the body-end compensation should give zero total geometric sextupole when integrating over the entire length of the magnet. In practice, however, this cancellation is not perfect. Also, the compensation is not working for all multipoles higher than the sextupole. The histogram in Figure 4 shows the distribution of sextupole in the machine after combining the end and body data obtained from the MTF measurement database [3], indicating a 1.47 unit b_2 average.
   Another characteristic of Tevatron dipoles (as can be noted in Table 1) is the large 18-pole (b_8). As will be shown later in section 5.0.), this multipole is mostly related to the fact that the high-field-quality region in the cross-section of Tevatron dipoles is extended further in horizontal than in vertical direction. This is very suitable for fixed target operation (which was the initial operational mode of the Tevatron ring).
   The production was continuously monitored and great care was taken to achieve balance between the body and end to achieve low average sextupoles. Note that this also applies to magnet assembly and magnet installation in the ring. The magnet positions in the ring were chosen such as to minimize the effect of the end sextupole.
   The average sextupole of all the Tevatron magnets produced as listed in Table 1 is 1.47 units, with a sigma of 3.09 units. The average sextupole of all dipoles built into the Tevatron ring, at flattop energy (or ~ 4000 A) is lower, namely ~0.8 units. This implies that the average width of the hysteretic loop at ~4000 A is 2·0.8 units. This could not be verified since the archive loops do not have enough data points to reconstruct the "turn-around" region of the loop. Although not discussed in further detail here, Table 1 also lists the average body, end and combined multipoles of all dipole magnets installed in the

Tevatron ring up to n=12. Note that the multipoles contained in the following table are the average over all dipoles currently installed in the ring.

Table 1: Mean and sigma of geometric multipoles (in units of 10^{-4} of the main dipole) in all Tevatron dipoles installed in the ring (see equ. 1 for notation). Up-stream end, down-stream end, body (center) and combined data from [3]. End and body data are combined according to equ. 2.

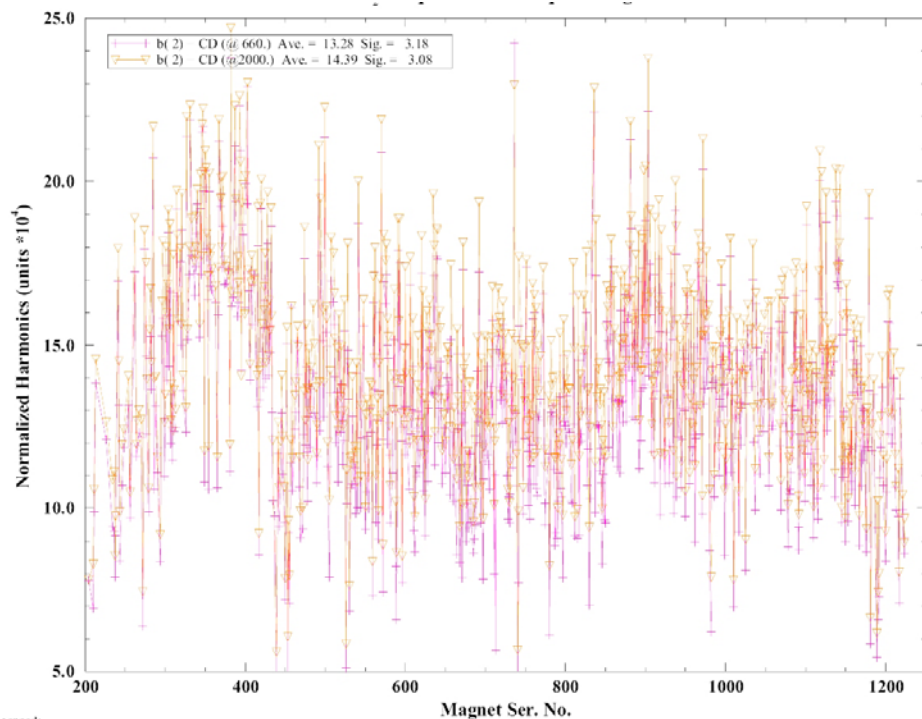|	Up - Down Ramp Average 2000A data											
	Combined			Position 'ED'			Position 'EU'			Position 'CD'		
	Ave	σ	No.	Ave	σ	No.	Ave	σ	No.	Ave	σ	No.
b_1	-0.06	0.76	770	-0.62	1.53	769	0.09	1.42	767	0.64	0.92	764
b_2	1.47	3.09	768	-6.79	3.22	769	-6.92	3.2	769	14.39	3.08	764
b_3	-0.26	0.76	770	-0.39	0.89	769	-0.18	0.86	767	-0.15	0.83	764
b_4	-0.13	1.2	770	-0.93	1.23	769	-1.09	1.41	767	1.83	1.23	764
b_5	-0.05	0.32	770	-0.05	0.33	769	-0.09	0.35	767	-0.03	0.37	764
b_6	4.98	0.51	770	4.86	0.55	769	4.76	0.59	767	5.28	0.54	764
b_7	0.02	0.15	770	-0.09	0.24	769	0.05	0.13	767	0.16	0.29	764
b_8	-12.3	0.34	770	-12.22	0.41	769	-12.31	0.4	767	-12.46	0.4	764
b_9	0.04	0.26	770	0.06	0.36	769	-0.12	0.32	767	0.1	0.43	764
b_{10}	3.66	0.26	770	3.62	0.36	769	3.58	0.31	767	3.76	0.4	764
b_{11}	-0.04	0.22	770	-0.08	0.31	769	0.16	0.28	767	-0.11	0.33	764
b_{12}	-0.82	0.21	770	-0.81	0.31	769	-0.78	0.25	767	-0.84	0.3	764
a_1	0.01	0.94	770	-0.28	1.78	769	-0.22	1.56	767	0.48	1.03	764
a_2	-0.06	1.23	770	0.47	1.57	769	-0.21	1.55	767	-0.09	1.23	764
a_3	-0.07	1.44	770	-0.09	1.51	769	-0.08	1.53	767	-0.08	1.46	764
a_4	-0.14	0.45	770	-0.18	0.54	769	0.01	0.47	767	-0.06	0.51	764
a_5	-0.11	0.3	770	-0.09	0.39	769	-0.18	0.4	767	-0.04	0.4	764
a_6	-0.11	0.3	770	-0.09	0.39	769	-0.18	0.4	767	-0.04	0.4	764
a_7	0.21	0.25	770	0.22	0.29	769	0.18	0.2	767	0.22	0.31	764
a_8	-0.02	0.42	770	-0.03	0.66	769	0.07	0.64	767	-0.04	0.6	764
a_9	0.26	0.37	770	0.25	0.4	769	0.24	0.41	767	0.31	0.49	764
a_{10}	0.05	0.26	770	0.13	0.41	769	-0.04	0.37	767	0.04	0.4	764
a_{11}	-0.23	0.26	770	-0.21	0.34	769	-0.23	0.33	767	-0.25	0.36	764
a_{12}	-0.05	0.24	770	-0.12	0.37	769	0.08	0.28	767	-0.05	0.35	764

Figure 2: Up-Down ramp average of sextupole in the body of most of the installed Tevatron dipole magnets calculated from the 660 A and at 2000 A magnetic measurement points. The up-down average of the hysteretic b_2 is approximately the geometric b_2.
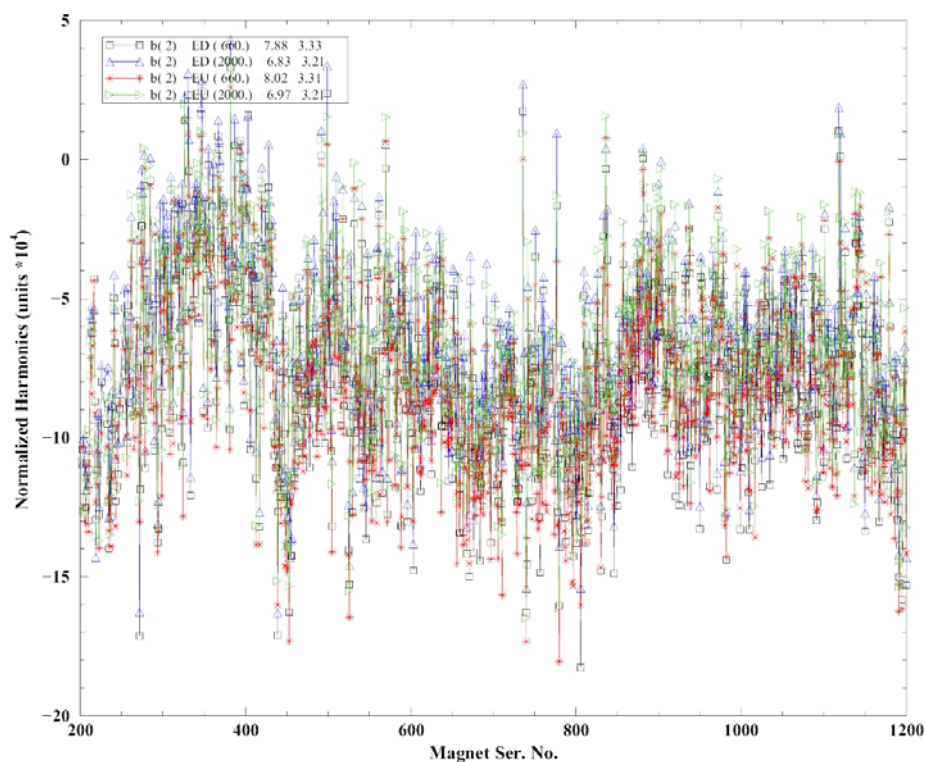

Figure 3: Up-Down ramp average of sextupole in most of the Tevatron dipole magnet ends (downstream and upstream) calculated from the 660 A and 2000 A magnetic measurement data. The up-down average of the hysteretic b_2 is approximately the geometric b_2.

Tevatron Dipole Harmonics Studies

UpDown Ave: b(2) AV (@2000.) Ser. 0200-1224

Average: 1.47
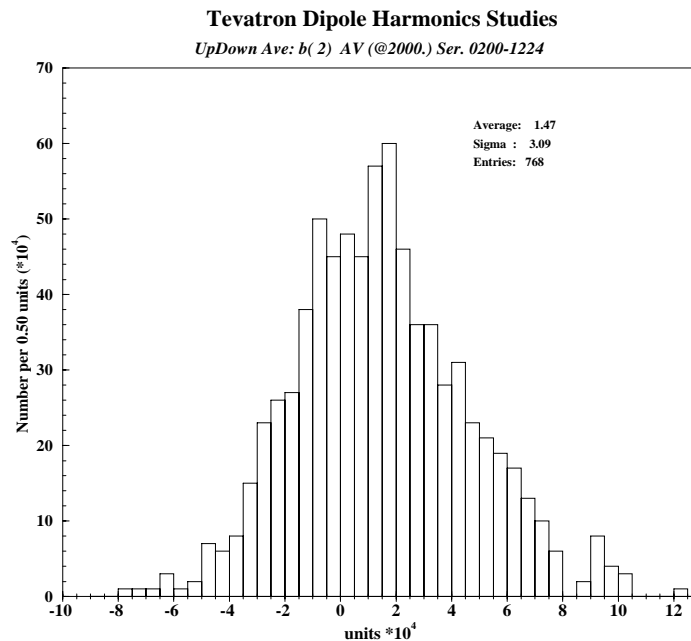Sigma :   3.09
Entries: 768

Figure 4: Geometric b_2 histogram for most of the 774 installed Tevatron dipoles (average of body and end and up-down data at 2000 A). End and body data were combined to yield the average sextupole. The average sextupole is 1.47 units. The distribution sigma is 3.09 units.

3)   2D Fields

Several different 2D models of the Tevatron dipole cross-section were generated: analytical models, finite element (FE) models using OPERA2D[2] and models using the numerical code Roxie[3] (with and without the FE option to calculate the effect of the iron yoke). A comparison of the analytical and FE shell models was made first in order to gain confidence in the FE codes (chapter 3.1.). The analytical models were also used in the sensitivity analysis presented in chapter 3.3.). FE and numerical models, in which the magnet coils are implemented on a turn-to-turn basis, were generated in OPERA2D and Roxie (chapter 3.2.). The numerical and FE models were used to compute the multipoles with better accuracy as well as to calculate iron yoke saturation effects. In addition the analytical model as well as the FE shell model were tuned such as to produce the same multipole content as the turn-by-turn implementations. As customary in the Tevatron the magnetic multipoles are quoted at a reference radius of 1" (25.4 mm).

3.1) Analytical vs FE 2D Models

Files: tev_v1_2_new (2 shell with simple yoke), tev_v1_3 (2-shell with simple yoke incl. bus and excl. radial insulation in coil mid- and pole-plane boundaries); Directory:

---

[2] Vector Fields Limited, England, OPERA2D™ and OPERA3D™
[3] S. Russenschuck, S, Kurz "Numerical Simulation of Superconducting Accelerator Magnets",
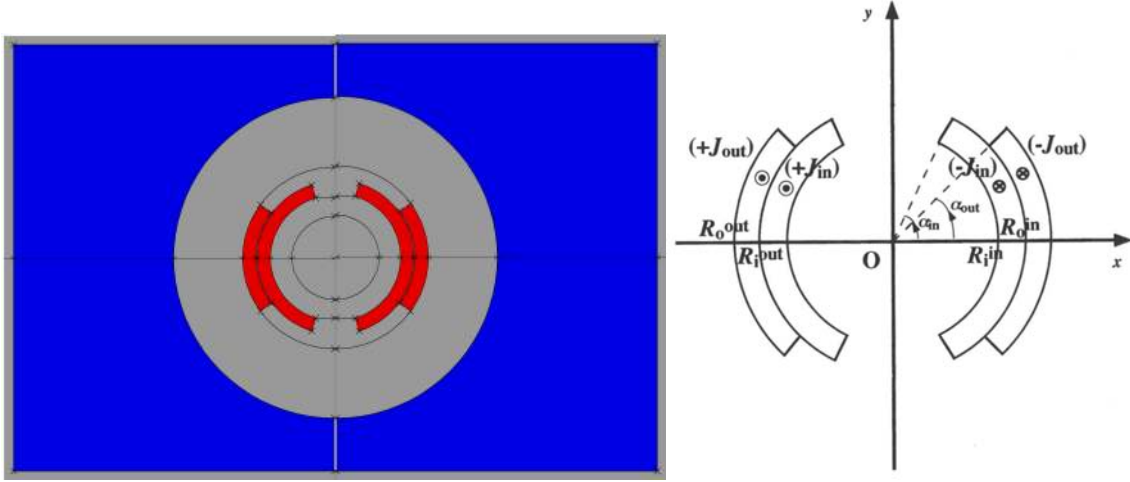IEEE Trans. Appl. Supercond.: 12 (2002) No. 1, pp.1442-1447

Figure 5: Left: simple FE model with shell-type coils; Right: Nomenclature of analytical model (according to [5]).

pb/tevatron/dipole1;

The simplest model of the Tevatron dipole cross-section consists of two current shells representing the coils, surrounded by a rectangular cross-section yoke with a circular inner boundary. The magnetic field produced by a current shell can be calculated analytically. The analytic formula ([5]) for the dipole field, B_0, and the higher allowed $2n$ multipoles, B_{2n}, produced by two current shells, including the field enhancement due to the iron is given in equations (3a) and (3b) (angles are in radians). Figure 5 shows a schematic of such a 2-shell model for the Tevatron dipole and includes the nomenclature for equ. 3. The iron effect is included in the analytical approximation using a magnetic

$$B_0 = \left\{ \begin{array}{l} \left[\dfrac{2\mu_0 j_{in}}{\pi}\left(R_o^{in} - R_i^{in}\right)\sin\alpha^{in} \right]\left[1 + \dfrac{\mu-1}{\mu+1}\left(\dfrac{R_o^{in} R_i^{in}}{R_{yoke}^2} \right) \right] + \\[4mm] \left[\dfrac{2\mu_0 j_{out}}{\pi}\left(R_o^{out} - R_i^{out}\right)\sin\alpha^{out} \right]\left[1 + \dfrac{\mu-1}{\mu+1}\left(\dfrac{R_o^{out} R_i^{out}}{R_{yoke}^2} \right) \right] \end{array} \right\} \tag{3a}$$

$$B_{2n} = \left\{ \begin{array}{l} \left[\dfrac{2\mu_0 j_{in} R_{ref}}{\pi(2n+1)(2n-1)}\left(\left(\dfrac{R_{ref}}{R_i^{in}}\right)^{2n-1} - \left(\dfrac{R_{ref}}{R_o^{in}}\right)^{2n-1} \right)\sin\left((2n+1)\alpha^{in}\right) \right]\left[1 + \dfrac{\mu-1}{\mu+1}\left(\dfrac{R_o^{in} R_i^{in}}{R_{yoke}^2} \right)^{2n+1} \right] + \\[4mm] \left[\dfrac{2\mu_0 j_{out} R_{ref}}{\pi(2n+1)(2n-1)}\left(\left(\dfrac{R_{ref}}{R_i^{out}}\right)^{2n-1} - \left(\dfrac{R_{ref}}{R_o^{out}}\right)^{2n-1} \right)\sin\left((2n+1)\alpha^{out}\right) \right]\left[1 + \dfrac{\mu-1}{\mu+1}\left(\dfrac{R_o^{out} R_i^{out}}{R_{yoke}^2} \right)^{2n+1} \right] \end{array} \right\}$$

$$\tag{3b}$$

mirror model, which assumes a constant permeability $(\mu=1000)$ iron yoke that stretches from a circular inner boundary (at R_{yoke}) towards infinity. The average current density in the shells is computed from the current per turn, the number of turns in and the total area of the shell. A comparison of the analytical, FE shell and numerical Roxie implementations of the two-shell model was performed first to gain confidence in the models.

   Rough approximations of the magnet geometry parameters were taken from [1] and [4]. They were further fine tuned to produce approximately the multipole content of the average Tevatron dipole listed in Table 1. The most important geometric model parameters are the shell pole angles (α^{in} in the inner layer, α^{out} in the outer layer): They are quoted as 72.94º and 36.48º in [4], and as 72º and 36º in [1]. The discrepancy in the quoted angles is believed to be representative of typical variations in the produced magnets. The angles used in the simulations presented here were those automatically computed with Roxie assuming a design where the outer layer cable has the same insulation thickness as the inner layer (and assuming that the bus turn is not different from the other turns). Using the parameters listed in Table 2 the 2D multipoles were computed with the analytical model, Roxie 9.0 and OPERA2D. Note that the angles and radii quoted in Table 2 are boundaries of the naked coils. Figure 6 shows the field-map obtained with OPERA2D for the injection case. The OPERA2D model included a realistic implementation of the iron yoke, with the default OPERA2D B-H curve for its magnetic properties. The Roxie 9.0 model used the analytical iron mirror model $(\mu=1000)$.

   The main dipole field B_0 calculated with the different models agree to within 1 %. The computed fields are given in Table 3. The higher order multipoles, listed in Table 4 also agree to a reasonable level of accuracy. Note that the Roxie model uses a turn-by-turn implementation and not shells.

Table 2: Shell model parameters, Subscript i / o stand for inner/outer;

Inner shell
final ("bare") angle α^{in}: 73.14º
bare conductor inner edge R_i^{in}: 38.2 mm
bare conductor outer edge R_o^{in}: 45.4 mm
Outer shell
final ("bare") angle α^{out}: 36.66º
bare conductor inner edge R_i^{out}: 46.1 mm
bare conductor outer edge R_o^{out}: 53.3 mm
Yoke
inner radius R_{yoke}: 95.63 mm
Vertical outer boundary R_{yoke}^x=190.5 mm
Horizontal outer boundary R_{yoke}^y =127 mm
Current density (injection)
$j_{in}=j_{out}$
j_{out} =21·666A·1/(((π36.66º/(2·180º))(53.3²-46.1²))=61.1 A/mm²

Table 3: Peak and bore fields in Tevatron dipoles at injection/collision computed with OPERA.

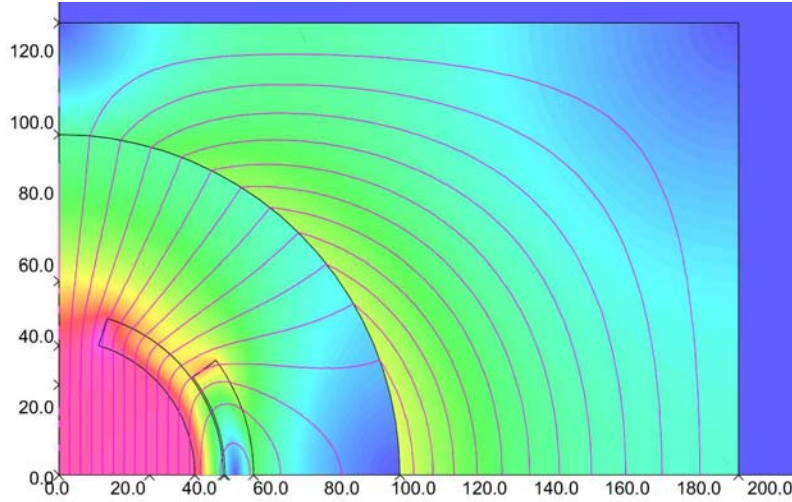| Field (T)	Injection (150 GeV, 666 A)	Collision (980 GeV, 4333 A)
peak	0.750	4.876
bore	0.666	4.335

Figure 6: Calculated OPERA2D field map of quadrant I of the Tevatron dipole at injection.

Table 4: Main dipole (in T) and higher multipoles (in units of 10^{-4} of the main dipole) components in Tevatron dipoles, calculated with OPERA2D, Roxie 9.0 and analytically (equ. (3)) as compared to the average measurement from the data archive ("position CD"). The multipole index n is according to the US notation (corresponding to the 2n+2 pole).

multipole n	0 (T)	1	2	3	4	5	6	7	8	9	10
OP2Dshell	0.658	0	22.7	0	13.1	0	5.6	0	-12.0	0	4.2
Roxie 9.0	0.666	0	27.8	0	8.5	0	5.8	0	-12.1	0	4.3
analytical	0.667	0	24.1	0	10.4	0	5.2	0	-11.9	0	4.2
archive (ave)	0.666	0	14.4	-0.1	1.8	0	5.3	0.2	-12.5	0.1	3.8

3.2) Turn-by-Turn 2D Models

   More refined implementations of the cross-sectional geometry than discussed above are required to obtain more accurate estimates of the field quality. OPERA2D and Roxie (7.0 & 9.0) models were prepared to reflect the coil geometry on a turn-by-turn basis. The analytical and FE shell models introduced in 3.1) were modified to replicate the results of the turn-by-turn models. The OPERA2D model was used to calculate saturation effects and is discussed further in 3.4). The Roxie 7.0 model was entirely replaced by a new Roxie 9.0 model and therefore not discussed any further here. The Roxie 7.0 model, however, was used in the sensitivity analysis in chapter 3.3).

The OPERA2D models are: tev_v2_1 (72.94º, 36.348º), tev_v2_2 (72º, 36º), tev_v2_3 (72.5º, 36.186º) in pb/tevatron/dipole2;
The Roxie7.0 model is called s2d_tevdip_3 in pb/tevatron/dipole3;
The Roxie 9.0 model is called s2d_tevdip_R90_Feyoke_opti in pb/Tevatron/dipoleR90/Tevdip_R90_2D;
The simple FE shell model is called tev_v1_3. in pb/tevatron/dipole1;
The analytical model is Tevatron_dipole_B2D_analytic_complexshell.mcd in pb/tevatron/dipole1;

Roxie stacks the cables according to a cable cross-section template and a specified azimuthal insulation thickness. The cable dimensions in the Roxie-model are given in Table 6. Note that the azimuthal insulation thicknesses in the inner and outer layers were assumed to be different (the outer layer being more compact). Roxie 9.0 uses a FE implementation of the iron yoke, so the correct shape of the iron yoke was implemented. Table 6 contains all the model parameters. The analytical shell model represents the "bare" coils. It was found that the thin layers of insulation bounding the coils azimuthally in the mid-and pole-planes had to be "current-free" in the shell models to achieve good agreement with the turn-by-turn models. Since the azimuthal turn-to-turn insulation cannot be extracted from the shell in the simple shell model the current density was reduced, thus distributing the current over the cable including the azimuthal insulation (excluding the first layer of insulation in the mid-and pole-planes). All models also included the outer layer mid-plane bus turn, which has a thicker insulation. In particular it was found that the analytical model could be made to agree well with the turn-by-turn models if the lower current density in the outer-layer mid-plane due to the thick bus-turn insulation is taken into account. The particularities of the coil geometry implementation of each model lead to slight differences in the pole angles and cable cross-sections. These differences, however, are not important, and smaller than the coil size variations obtained in magnet mass-production, as evidenced by the large width (σ of several units) of the multipole distributions quoted in Table 1.

Table 5 shows that the field computations with the different models agree reasonably well. As intended the 2D geometric multipoles in the body of the Tevatron dipole magnets calculated with the above discussed models are in good agreement with the average measured body b_2 in the Tevatron dipoles. Also, a comparison with the results obtained with simpler models, as reported in Table 4 reveals that the more realistic implementation of the coils produces ~5 units of b_2 less. This is mostly the result of the insulation in the mid-plane (~135 μm in inner layer). Especially in the outer layer the bus has a 0.4 mm insulation. Figure 7 shows the field distribution in the coils computed with the Roxie 9.0 turn-by-turn implementations.

Table 5: Multipoles (in units of 10^{-4} of the main dipole) in Tevatron dipoles, calculated with Roxie 9.0 and the "adapted-to-fit" analytical model. The models used the geometry parameters specified in Table 6. The main field at injection is given in Tesla. The multipole index n is according to the US notation (corresponding to 2n+2 pole).

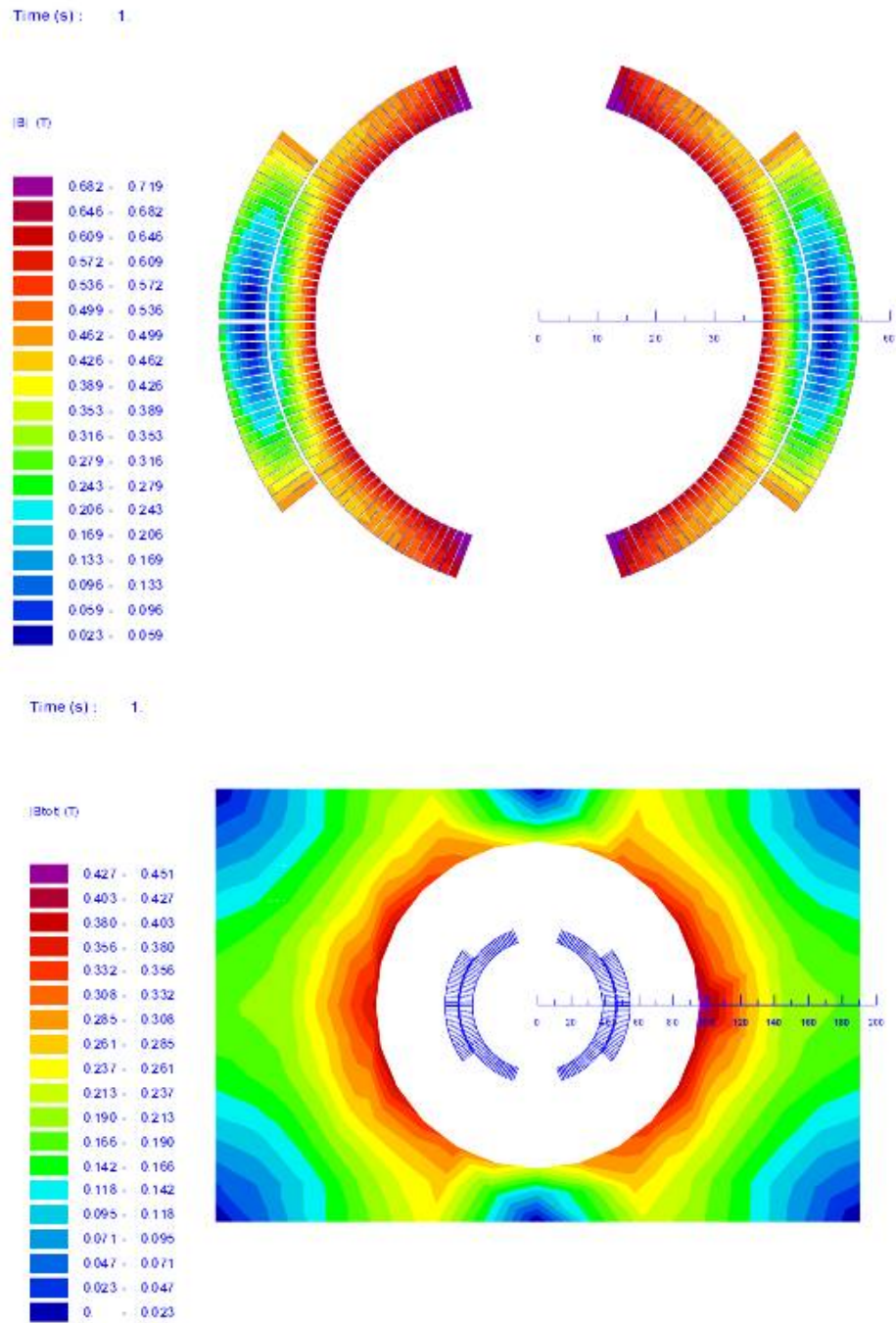| multipole	0 (T)	1	2	3	4	5	6	7	8	9	10
Roxie 9.0	0.666	0	12.9	0	2.1	0	4.4	0	-12.3	0	4.2
analytical ("adapt.")	0.666	0	14.2	0	2.0	0	4.1	0	-12.4	0	4.3
archive (ave)	0.666	0	14.4	-0.1	1.8	0	5.3	0.2	-12.5	0.1	3.8

Figure 7: Roxie 9.0 field distribution in the body of
the Tevatron dipole (coils left, yoke right).

Table 6: Tevatron dipole, magnetic cross-section model parameters; Angles and radii represent the "naked" coil boundaries (wout insulation); * Roxie 9.0 options: -a- inner edge alignment, -b- radial grading of current density, -c- current filamentation parameters: N1=1, N2=9, -d- without thermal contraction option;

Parameter	Roxie 9.0*	Analytical
Inner Layer		
starting angle α_i^{in}	0.2º	0.1º
final angle α_o^{in}	73.14º	73.06º
inner radial edge R_i^{in}	38.2 mm	38.2 mm
outer radial edge R_o^{in}	45.4 mm	45.1 mm
number of turns	35	35
turn arrangement	"true"	shell, mid&pole wedges
cable bare inner thickness	1.127 mm	-
cable bare outer thickness	1.377 mm	-
cable bare width	7.198 mm	6.898 mm
azimuthal insul. thickness	134.5 µm	-
radial insul. thickness	100µm	-
cable curr. dens. @ 666 A	-	63.7 A/mm^2
Outer layer		
starting angle α_i^{out}	2.5º	2.0º
final angle α_o^{out}	36.66º	37.36º [1]
inner edge R_i^{out}:	46.1 mm	45.8 mm
outer edge R_o^{out}	53.3 mm	52.7 mm
number of turns	20	20
turn arrangement	"true"	shell, mid&pole wedges
cable bare inner thickness	1.127 mm	-
cable bare outer thickness	1.377 mm	-
cable bare width	7.198 mm	6.898 mm
azimuthal insul. thickness	127 µm	-
radial insul. thickness	101µm	-
cable curr. dens. @ inject.	-	63.5 A/mm^2
Bus		
starting angle α_{bus}^{out}	0.5º	0.3º
final angle α_{bus}^{out}	2.0º	1.7º
inner edge R_i^{out}:	46.1 mm	45.8 mm
outer edge R_o^{out}	53.3 mm	52.7 mm
number of turns	1	1
turn arrangement	"true"	shell, mid&pole wedges
cable bare inner thickness	1.127 mm	-
cable bare outer thickness	1.377 mm	-
cable bare width	7.198 mm	6.898 mm
azimuthal insul. thickness	0.400 mm	-
radial insul. thickness	101µm	-
cable curr. dens. @ inject.	-	80.2 A/mm^2
Yoke		
inner radius R_{yoke}	95.63 mm	95.63 mm
horizontal outer bound R_{yoke}^x	190.5 mm	∞
vertical outer bound R_{yoke}^y	127 mm	∞
BH-curve	ROXIE-default (LHC)	µ=1000

3.3) Geometric 2D Multipole Variation and Sensitivity Analysis

The "adapted" analytical shell-model, which includes a separate implementation of the bus and the mid-plane insulation in the inner layer (see discussion in 3.2.), was used to estimate the effect of pole and mid-plane angle variations on the cross-section multipoles. An "asymmetric" implementation of the coil in Roxie 7.0 (the Roxie 7.0 model uses a circular, infinite, constant permeability iron mirror model) was used to estimate the effect of up-down and left-right asymmetries as well as the effect of coil de-centering in the yoke (*a2d_tevdip_2 in pb/tevatron/dipole4*). The following reports the results of the sensitivity studies.

   Pole-angle variation along the production history is the most likely cause of multipole variation in Tevatron coils. The most important cause is a (sometimes deliberate) variation in azimuthal coil pre-stress (pole-plane shimming), cable size and insulation thickness. The estimated effect of a 1º (or more precisely ± 0.5º from "standard") variation of pole angle on the sextupole is almost 30 units, a large amount. Given that the outer coil spans approximately half the angle of the inner coil, the analysis assumed a 0.5º (or more precisely ± 0.25º from "standard") variation in the pole angle of the outer coil. Table 7 summarizes the result of the angle variations within the above indicated b_2 range. The equilibrium or "standard" angle was assumed to be the angle that was implemented in the models discussed in 3.1) and 3.2). The outer coil pole angle was varied exactly half as much as the inner coil pole angle. A 0.5º variation in the inner layer pole-angle corresponds to a azimuthal coil size variation of 0.35 mm.

Table 7: Analysis of pole-angle effects on the geometric b_2 (in units) in the body straight section of the Tevatron dipoles. The 0º angles refer to 72.385º / 36.193º in the inner / outer layer pole angles (bare coil boundary in pole region). All other model parameters such as stated in Table 6.

outer↓/inner→	-0.5º	0º	+0.5º
-0.25º	30.5	19.5	8.9
0º	25.8	14.8	4.2
+0.25º	21	17.9	-0.6

   Another important coil geometry parameter is the mid-plane shimming. The outer coil mid-plane turn in quadrant I is the Tevatron bus, which has a thick (~0.4 mm) insulation. Therefore all other quadrants are shimmed in the mid-plane outer layer to prevent asymmetry. As shown in the following a variation in shimming of the order of 0.2º (or ~150 μm) can result in b_2-variations of more than 10 units if the pole-angles remain unchanged (Table 8) and up to 20 units if the pole-angles change at the same rate as the mid-plane angles (Table 9). The rule of thumb is that ~1 mrad of mid-plane shimming in both layers (assuming that the pole angle follows) produces ~1 unit in b_2.

   The asymmetric Roxie model was used to model the effect of horizontal and vertical de-centering of the coils within the yoke. The asymmetric model before the transformations is similar to the symmetric model reported in part 3.2). Table 10 reports the effect of the main vertical and horizontal asymmetry modes on the major multipoles.

Table 8: Analysis of mid-plane angle effects on the geometric b_2 (in units) in the body straight section of the Tevatron dipoles. The 0º angles refer to 0.375º / 0.5224º in the inner / outer layer pole angles (bare coil boundary in mid-plane). The ("bare") pole-angles were fixed at 72.385º and 36.193º in this simulation. All other model parameters are such as stated in Table 6.

outer↓/inner→	-0.2º	0º	+0.2º
-0.2º	25.3	17.4	9.4
0º	22.7	14.8	6.8
+0.2º	20.1	12.2	4.1

Table 9: Analysis of mid-plane angle effects on the geometric b_2 (in units) in the body straight section of the Tevatron dipoles. The 0º angles refer to 0.375º / 0.5224º in the inner / outer layer pole angles (bare coil boundary in mid-plane). The pole-angles were changed according to the mid-plane angles from their "standard" ("bare") value of 72.385º and 36.193º in this simulation. All other model parameters are such as stated in Table 6.

outer↓/inner→	-0.2º	0º	+0.2º
-0.2º	33.5	21.2	2.5
0º	27.1	14.8	7.5
+0.2º	20.7	8.3	-4

Up-down asymmetries introduce skew quadrupole moments, left-right asymmetries introduce normal quadrupole moments. The higher order modes appearing together with them (e.g. a_3, a_5 or b_3, b_5) are usually negligible. Also the effect on the allowed harmonics is usually negligible, except for the sextupole b_2. The effect of some modes of asymmetric azimuthal coil-positioning errors and coil-size variations (not to be confused with the symmetric azimuthal size variations discussed in Table 7-Table 9) are shown in Table 11. These are azimuthal gaps in the mid-plane with up-down and left right asymmetry as well as asymmetric pole angle variations and rolls. Typically the transformations were chosen such as to produce 1 unit of normal (left-right asymmetry) or skew (up-down asymmetry) quadrupole.

   Summarizing it can be said that: –1- a vertical (horizontal) coil displacement in the yoke of ~100 μm produces ~1 unit of skew (normal) quadrupole; -2- a radial "blow-up" of the coil by ~250 μm produces ~1 unit of b_2; -3- 6 mdeg coil roll produce 1 unit of skew dipole; and -4- non-symmetric variations of the azimuthal coil sizes (upper-lower pole or left right) by 10 mdeg – 50 mdeg produce ~1 unit of normal or skew quadrupole.

Table 10: Effect of vertical and horizontal coil de-centering on the magnetic multipole distribution (at R_{ref}=25.4 mm, in units of 10^{-4} of the main field at injection). Simulations were performed with Roxie70 using a "linear iron" model. Only strongly (> 1 unit) changing multipoles are reported.
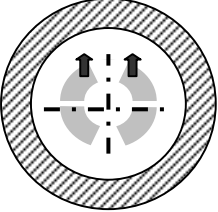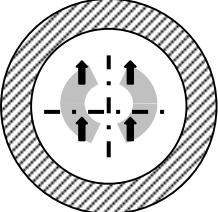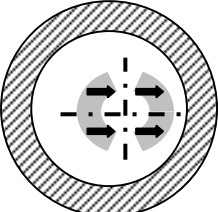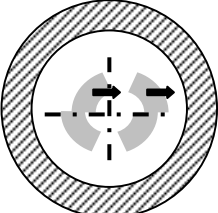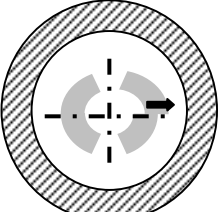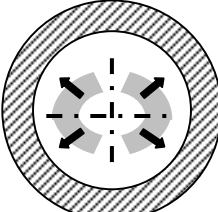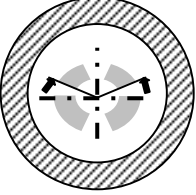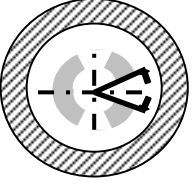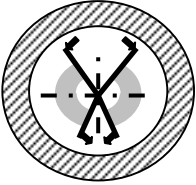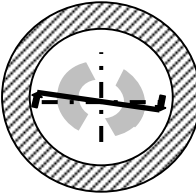
Transformation	Parameter	Multipole change
	Δy=0.18 mm	Δa_1=-1 Δb_2=-5.5
	Δy=0.085 mm	Δa_1=-1
	Δx=0.11 mm	Δb_1=-1
	Δx=0.22 mm	Δb_1=-1
	Δx=0.03 mm	Δa_1=1
	Δr=0.23 mm	Δb_2=-1

Table 11: Effect of asymmetric azimuthal coil size and positioning variations on multipole content of Tevatron dipoles. Simulations were performed with Roxie70 using a "linear iron" model (reference radius R_{ref}=25.4 mm, multipoles are quoted in units of 10^{-4} of the main field at injection). Only strongly (> 1 unit) changing multipoles are reported.

Transformation	*Parameter*	*Multipole change*
	inner layer only: $\Delta\phi$=0.08° outer layer only: $\Delta\phi$=0.05° both layers: $\Delta\phi$=0.03°	Δa_1=-1, Δb_2=-2 Δa_1=-1, Δb_2=-1 Δa_1=-1, Δb_2=-1.3
	symmetric: $\Delta\phi$=0.015° upper pole only: $\Delta\phi$=0.03°	Δb_1=-1, Δb_2=-0.7 Δb_1=-1, Δa_1=-0.5, Δb_2=-0.6
	$\Delta\phi$=0.012°	Δa_1=1
	$\Delta\phi$=0.005°	Δa_0=1

3.4) Saturation Effects

   The turn-by-turn OPERA2D and Roxie 9.0 models were used to calculate iron yoke saturation effects. Figure 8 shows a plot of the field distribution in the coils and the yoke as generated by one of the several OPERA2D turn-by-turn models (see the discussion in chapter 3.2). See Figure 7 for a similar plot obtained with Roxie. The yoke geometry implementation in the model corresponds to the yoke design in the Tevatron magnets. The results are presented in Table 12. The current densities in the turns were increased by a factor 4333/666 from injection to collision. Saturation effects appear to be weak, of the order of 0.2 units in b_2. They are entirely negligible in the case of the higher order multipoles.
. The OPERA2D turn-by-turn model achieves perfect radial stacking (with a cable that is not perfectly keystoned) by varying the thickness of the azimuthal turn-to-turn insulation with the radius. Perfectly radial stacking is, however, not achievable simultaneously in both layers with only one cable design such as is the case of the Tevatron dipole magnet.
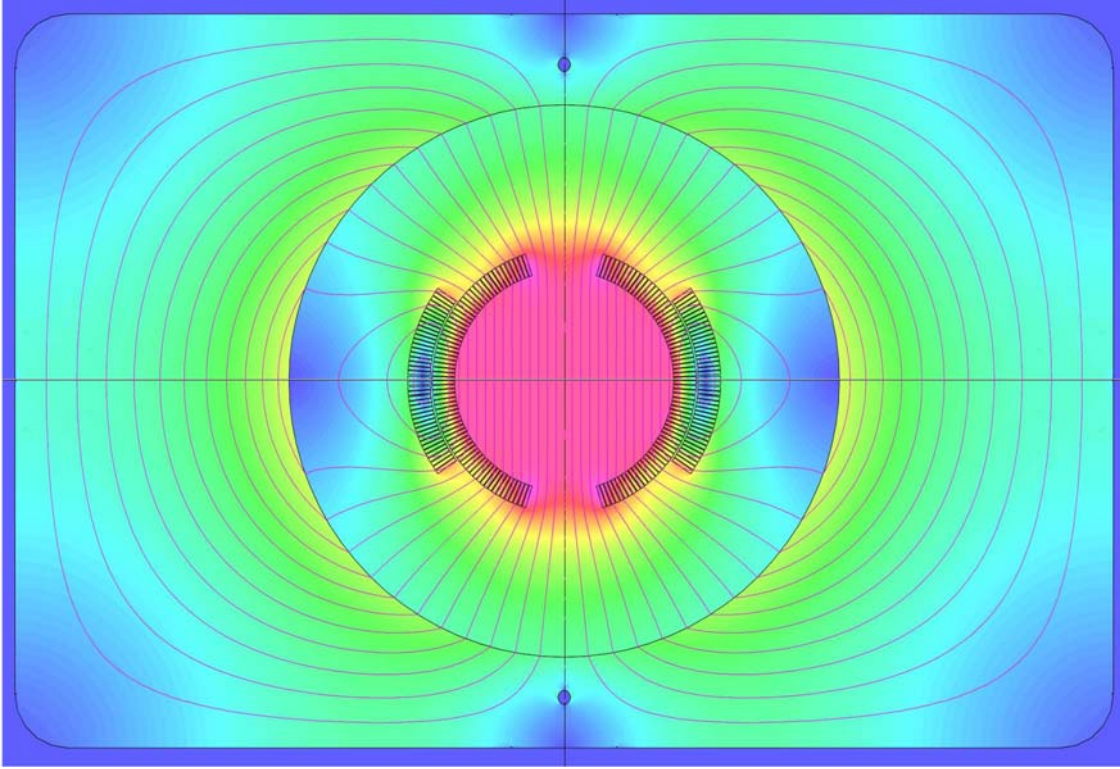
Figure 8: Field distribution in Tevatron dipole magnet at injection, as computed with OPERA2D. See Figure 7 for a similar plot computed with Roxie.

Table 12: Saturation effects in allowed multipoles in Tevatron dipoles, calculated with OPERA2D and Roxie 9.0. The numbers quoted represent the relative change of multipoles from injection to collision (in % of the injection value). The main field at injection / collision is 0.66T / 4.3T (see Table 3). The multipole index n is according to the US notation (corresponding to the 2n+2 pole).

n	2	4	6	8	10
OPERA2D	+1.9	0	0	0	0
Roxie 9.0	+1.4	-0.7	0	0	0

3.5) Transfer function

The transfer function calculated with Roxie 9.0 and the analytical model is 10 T/kA, very close to the "historic" value (i.e. the values measured routinely following magnet production) of 10 G/A. During Tevatron magnet production the transfer function was measured with NMR probes. The average transfer function of the 8 magnets measured is 10±0.1 G/A. The transfer function is linear within the operational range of the Tevatron dipoles (0-4350 A).

4)   3D Fields

All end field calculations were performed for a generic end, without leads and splices. The outer layer mid-plane turn, however, was extended beyond the end as a very crude attempt to simulate the leads and bus turn (see Figure 10). The effect of this model-parameter is, however, negligible. Although the Tevatron dipole end design is more or less straight forward and compact, there is a lack of precise geometry data, which made it difficult to reproduce the exact multipole content of the average Tevatron magnet end, such as quoted in Table 1. The procedure chosen was to fine-tune the end design such as to produce the same multipole as recently measured on magnet TB1055. The calculations were performed with the newly released Roxie 9.0 version, which includes FE modeling of the yoke using the BEM-FEM coupling method. The Roxie-files containing the model data are named *s3d_tevdip_R90_FEyoke_opti* and stored in *pb/tevatron/dipoleR90/TevdipR90_3D/Optimized_with_TB1055data*. As will be shown the multipole content of the ends found as a result of this procedure are also consistent with the average of all dipoles as measured after production. As is well known the complex multipole expansion (equation 1) is not valid in 3D fields such as in the ends (the length integrated multipole content is, however, invariant). Therefore the scaling law used to convert multipoles at one radial position in the bore to another doesn't apply. The comparison of the model and measurement data on TB1055 was performed at the radius of the measurement coils of 12.405 mm (see 4.2.). Once agreement was found, the fields were recalculated for the Tevatron reference radius of 25.4 mm (see 4.2.).

4.1) End-Field Model

A 3D magnetic model of the Tevatron dipole ends was generated with Roxie 9.0. As shown in Figure 9 the end-region is (arbitrarily) defined as the 50 cm long region, which begins 34.5 cm before the end of the yoke and ends 3.2 cm after the physical end of the coils. The end-multipoles given in Table 13 are the average multipoles over this 50 cm end region. To obtain the average, the numerical code integrates the fields over this end region and divides by its length. As discussed before the cross-sectional magnetic design included a small sextupole component to compensate for the strong negative sextupole generated in the magnet ends. The end-multipoles can be combined with the body multipoles to generate the total multipoles using the procedure outlined in 2.) and 4.3.). The comparison between the multipole data found here and the data measured and quoted in Table 1 will also be discussed in more detail in chapter 4.3. Figure 10 shows the Roxie 9.0 implementation of the coil-ends. Figure 11 shows the axial main field profile for two different currents. The equivalent magnetic length is also indicated. The equivalent magnetic length is defined as the "end" of the step-function that produces the same integrated dipole field. The model was tuned such as produce the average equivalent
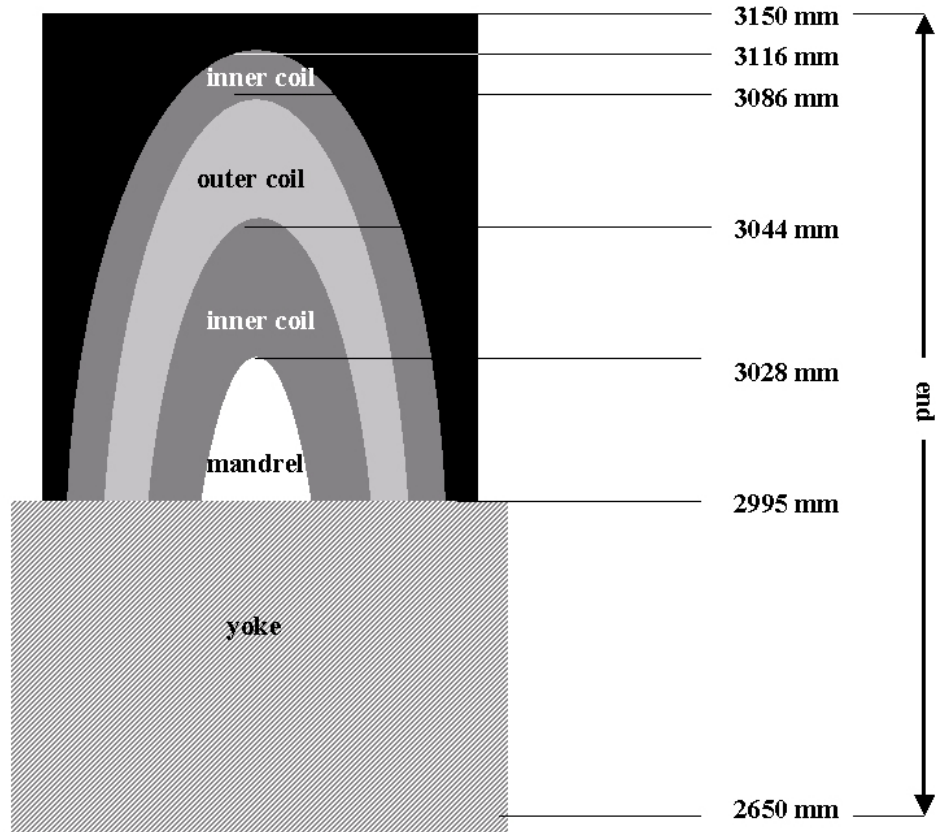
Figure 9: Schematic of average Tevatron ends (the model does not include leads), indicating the particular end length definition chosen here. The distances are quoted with respect to the magnet center.

magnetic length measured on all magnets produced - 6.116m [6]. Table 13 summarizes the end multipoles calculated with Roxie and normalized to the dipole field in the body. The evolution of the sextupole and decapole along the ends is shown in Figure 12. Similarly as in Table 13, the multipoles shown in Figure 12 are normalized on the dipole field in the straight section. Multipoles higher than n=4 are not discussed in any further detail here. They are shown in Figure 13.

Table 13: End multipoles in Tevatron dipoles at 1", calculated with Roxie 9.0. The multipolar field components were averaged over the 50 cm end section defined in Figure 9. The multipoles quoted are given in units of 10^{-4} of the body dipole field of 0.66 T at injection (666 A). The average end dipole is 0.579 T (at 666 A).

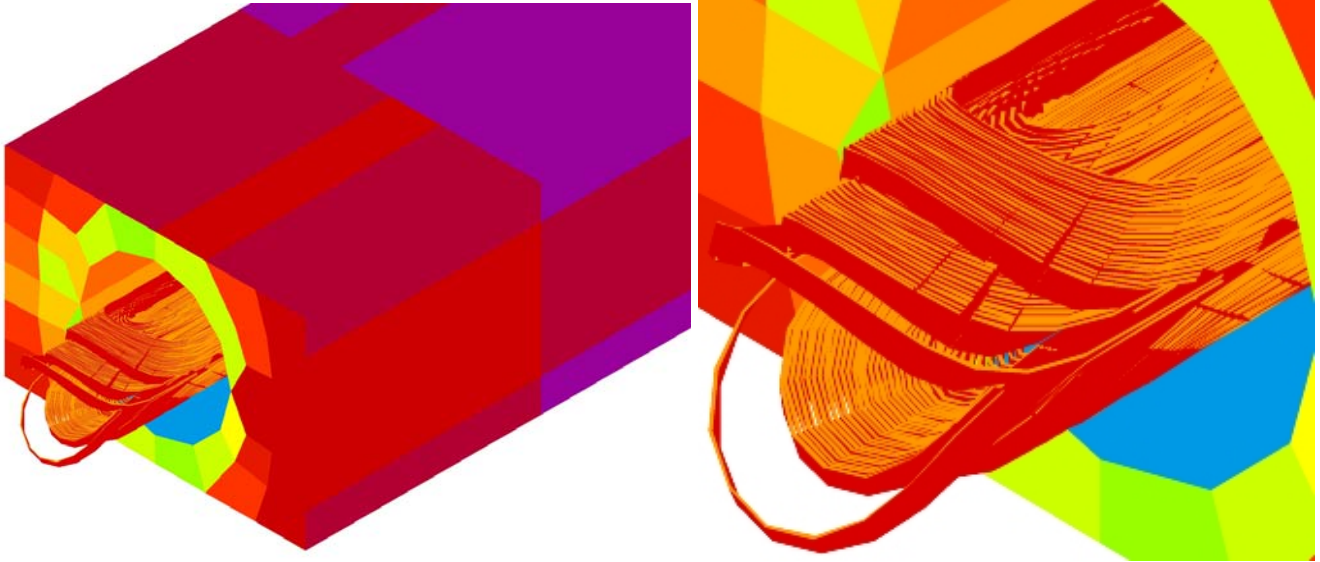| n	0	1	2	3	4	5	6	7	8	9	10
units	8690	0	-78	0	-12.7	0	1.4	0	-10.5	0	2.9

Figure 10: Roxie 9.0 BEM-FEM model of the end(s of the Tevatron dipole. The bus-turn (outer-layer – mid-plane turn) was pulled out further than the rest of the coils to simulate the leads. Left with yoke, right: detail of coil end (conductor naked – no insulation shown).
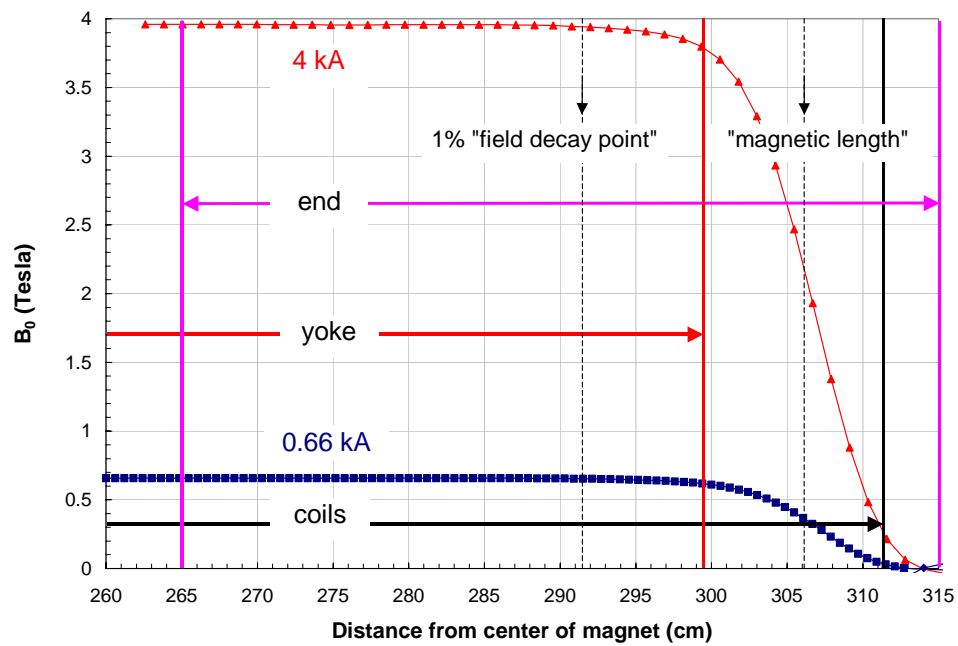

Figure 11: Axial field profile (normalized on cross-sectional field) for Tevatron dipole. The (arbitrary) definition of the ends used here is shown together with the yoke and (inner) coil delimitations. The axial dimension is the distance from the magnet center. Also shown is the equivalent step-function dipole field profile, indicating an equivalent magnet half-length of 3.058 m.
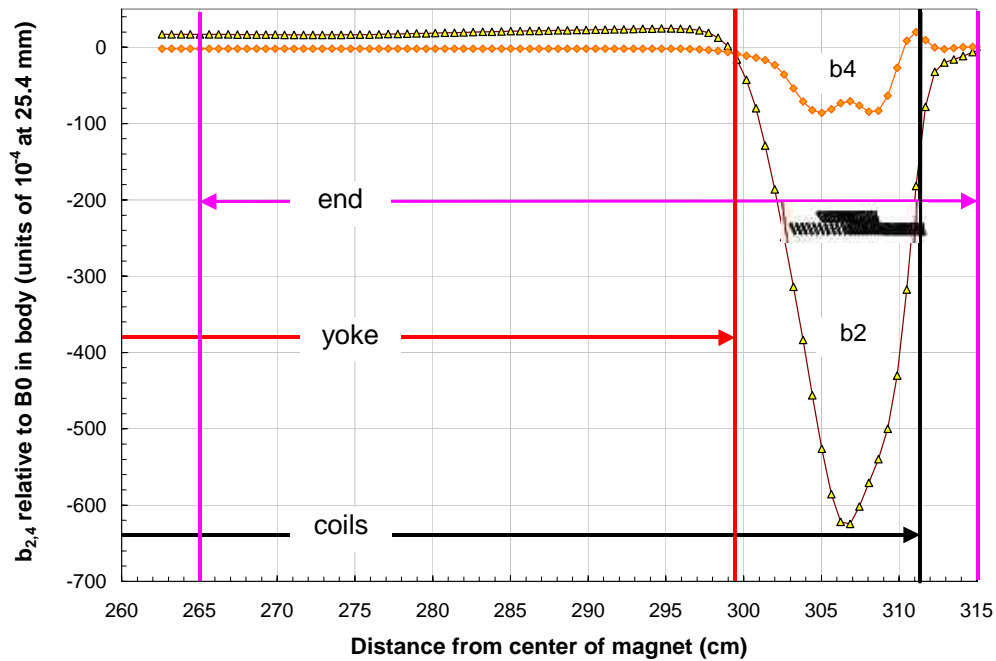
Figure 12: Profiles of sextupole and decapole in Tevatron dipole magnet vs distance from the magnet center. The definition of the ends used here is shown as well as the yoke and coil limits. The sextupole has a strong negative spike in the coil end region. The multipoles are given in units of 10^{-4} of the main dipole in the straight section (reference radius = 25.4 mm).
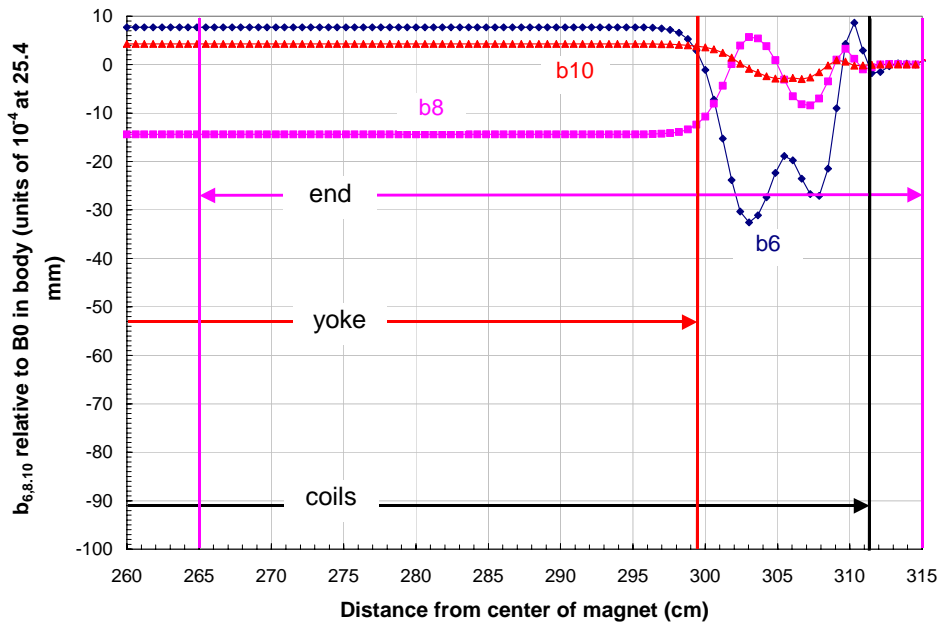

Figure 13: Profiles of high order multipoles in Tevatron dipole magnet vs distance from the magnet center. The definition of the ends used here is shown as well as the yoke and coil limits. The 14- and 22-pole are almost unchanged throughout the body and the ends. The multipoles are given in units of 10^{-4} of the main dipole in the straight section (reference radius = 25.4 mm).

4.2) Comparison with Measurement on TB1055

The Roxie 9.0 3D model of the Tevatron dipole end presented above was fine-tuned via a comparison to experimental data obtained in the Tevatron dipole TB 1055. A z-scan of the end fields was performed with a short (~ 4 cm) rotating coil probe at two different occasions in the lead end of TB1055. The probe sampled the bore field at a radius of 12.405 mm. The breakdown of the complex field expansion (equ. 1) in 3D fields makes scaling from one radial multipole distribution to another impossible. Therefore the model data were calculated at the same radius at which the measurements were obtained. Figure 14 shows a comparison of the dipole field at 4 kA. The agreement is reasonable in terms of the dipole strength. The model and experimental data, however, are shifted with respect to the position along the magnet. As discussed above, the coil length of the Roxie model as well as the exact position of the "end-bend" was chosen such as to fit the well-known magnetic length of the Tevatron dipoles (see "magnetic length" mark in Figure 14). The discrepancy is most likely related to an uncertainty in the probe position during the z-scan measurement. Figure 15 and Figure 16, which show the comparison of the calculated and experimental b_2 and b_4 data, obviously suffer from the same discrepancy. The graphs, however, show that the model was successfully fine-tuned on the measured results. As will be discussed next the end model data also agree well with the "average" end as derived from the archival magnetic measurement data.
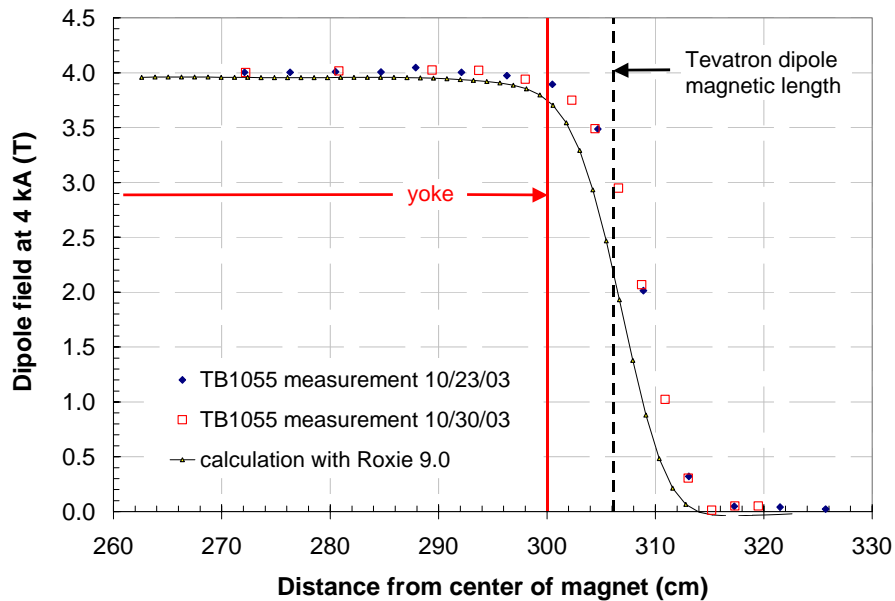

Figure 14: Comparison of Roxie 9.0 model with z-scan rotating coil measurement in magnet TB1055. Also shown is the edge of the magnetic yoke and the "magnetic length" of the Tevatron dipoles derived from the field integral measurements of all dipoles. The coil ends in the Roxie model were shifted in z such as to produce a field profile, which is consistent with the 6.116 m total magnetic length of the Tevatron magnets. The fact that the measured magnetic length of TB1055 is longer is most likely the result of an offset in the position of the measurement system.
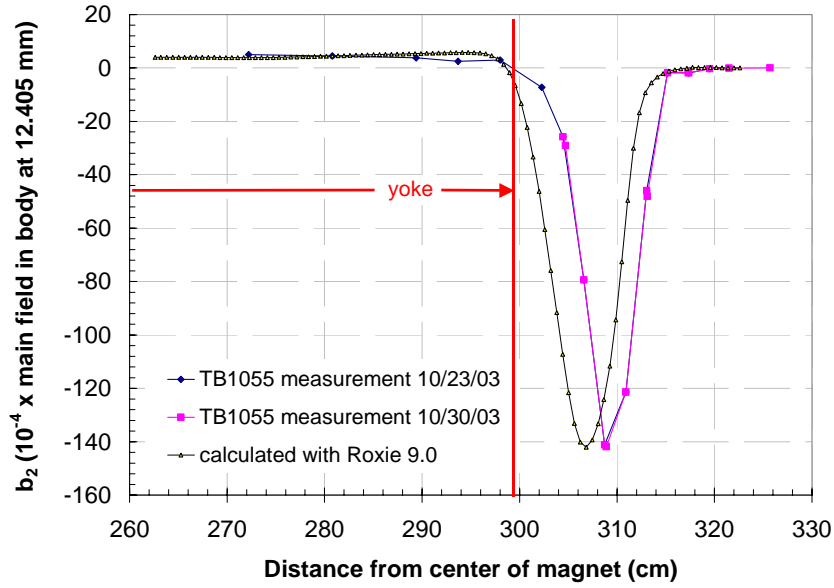
Figure 15: Comparison of Roxie 9.0 model with z-scan rotating coil measurement in magnet TB1055. Shown is the b_2 multipole along the end at the measurement radius of 12.405 mm. The Roxie-model was fine tuned to agree with the experimental data. The discrepancy of the position of the b_2 spike is most likely the result of an offset in the position of the measurement system. The coil ends in the Roxie model were shifted in z such as to produce a field profile, which is consistent with the 6.116 m total magnetic length of the Tevatron magnets.
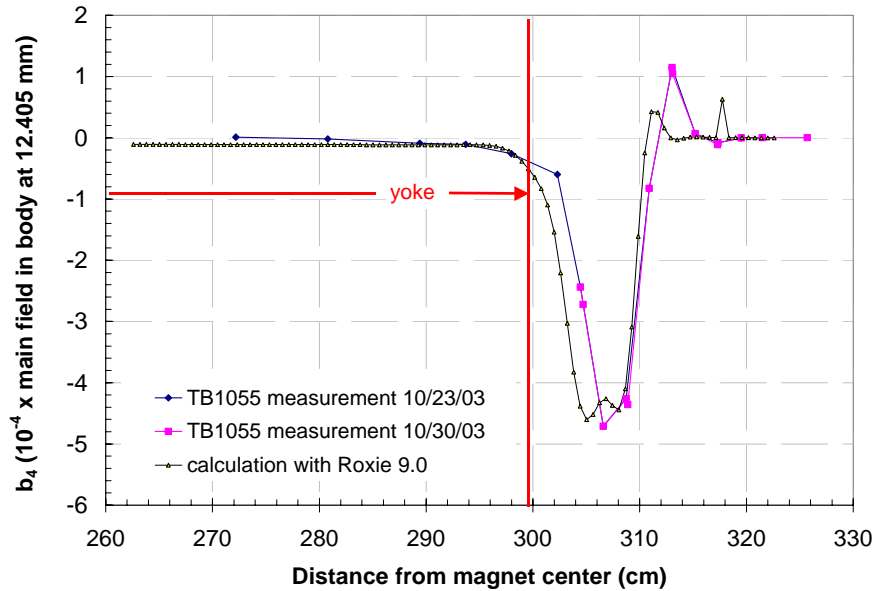

Figure 16: Comparison of Roxie 9.0 model with z-scan rotating coil measurement in magnet TB1055. Shown is the b_4 multipole along the end at the measurement radius of 12.405 mm. The Roxie-model was fine tuned to agree with the experimental data. The discrepancy of the position of the b_2 spike is most likely the result of an offset in the position of the measurement system. The coil ends in the Roxie model were shifted in z such as to produce a field profile, which is consistent with the 6.116 m total magnetic length of the Tevatron magnets.

4.3) Comparison with Archive Data

The axial multipole profiles shown in Figure 11-Figure 13 were calculated with the coil-end Roxie model discussed above. Figure 9 shows the limits of the above defined, 0.5 m, end region. The following discusses how the model data presented in 4.1.) can be compared to the magnetic multipole data of the "average" Tevatron dipole summarized in Table 1. For this purpose one approximates the longitudinal field profile with a step function, as shown in Figure 17. Knowing the standard amplitude of the rotating coil end field measurements in the "average" Tevatron dipole magnet, the exact position of the magnetic measurement probe in the case of the end measurement can be reconstructed. Unfortunately the standard amplitudes of the measurement of the "average" magnet is not known exactly (since the "average" magnet does not "exist" and was never measured). What we know are "typical" standard amplitudes obtained during the rotating coil measurements on the Tevatron dipoles: ~5700 au in end vs. ~7000 au in body measurement. As shown in equation (4) these numbers can be used to derive the "active" length, $L_{activeprobe}$, of the 95" measurement coil in the end measurements (which led to the data in Table 1). Note that the "active" length is defined with respect to the step magnetic field profile.

$$L_{probe}^{active} \sim \frac{57}{70} L_{probe} = 1.965\,m \tag{4}$$

Placing the measurement-coil into the end of a Tevatron dipole magnet such that 1.965 m of it is within the equivalent magnetic "half-length" of 3.058 m, it can be inferred that the rotating coil reached into the magnet to the 1.093 m mark from the center of the magnet. Furthermore it can be inferred that the end measurement probe was sticking out from the "equivalent magnet end" by 0.448 m, or 0.39 m from the physical end, given the 5.8 cm distance between the physical end of the coils and the end of the "equivalent length". (Figure 9). The multipolar data shown, e.g. in Figure 12 can now be integrated from 1.093 m from the center of the magnet to the end of the probe. In addition the data have to be normalized to the active probe length. Equation (5) gives the integration ($z=0$ is in the magnet center) and averaging procedure required to compute the magnet multipoles in the same convention that is used in Table 1 from the model field calculation in Roxie. The multipoles have to be defined with respect to the straight section field, e.g. 0.66 T at injection.

$$b_n^{end} = \frac{1}{L_{probe}^{active}} \left[\int_{1.093m}^{\infty} \left(\frac{B_n(z)}{B_{0,straight}} \right) dz \right] \tag{5}$$

b_n^{end} are the end multipoles according to the same convention that is used in Table 1, B_n is the nth multipolar field strength (T) and $B_{0,straight}$ is the dipole strength in the straight section. Table 14 lists the multipoles converted from the Roxie model using this procedure and compared to the data from Table 1.

Table 14: Comparison of measured and calculated end multipoles. The simulated end multipoles were converted to the convention used to tabulate the measured multipoles in Table 1.

n normal	measured u-end from Table 1	calculated end converted with (4&5)
2	-6.9	-6.4
4	-1.34	-4.8

As mentioned before, the longitudinal multipole profile for the "old" magnetic measurement data (as quoted in Table 1) is a step profile. Such a profile is shown in
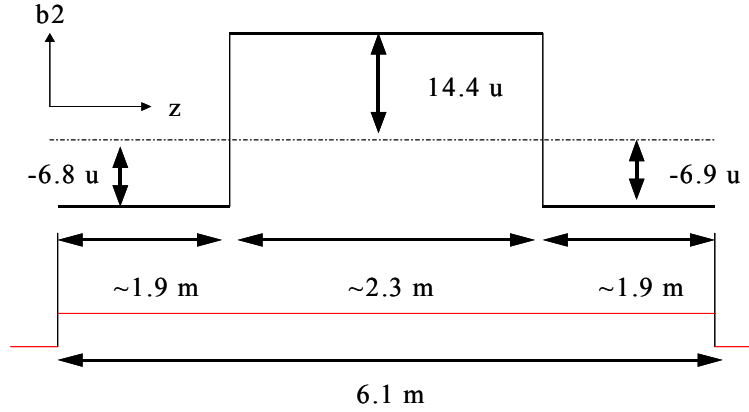

Figure 17: "Equivalent" step profile for the understanding of the magnetic measurement data quoted in Table 1.

Figure 17. The respective lengths of the end and body regions vary from magnet to magnet (depending on the exact positioning of the magnetic measurement probe within the magnet). The active probe lengths (for the two ends and the body) were calculated on the basis of some (remembered) set of standard amplitudes, which (as discussed before) are not necessarily representative of the "average" magnet under discussion here. Therefore the indications given in the plot are only approximate. For example: solving the b_2 length integral for the profile shown in Figure 17 yields an average combined b_2 of 1.16 instead of 1.47 predicted in the summary Table 1. Note that the comparison in Table 14, especially with regard to b_2 nevertheless confirms that the Roxie end simulation presented here is representative of the "average" magnet.

5)   Cross-sectional Field Profiles

Based on the body-end combined multi-polar content of the "average" Tevatron dipole given in Table 1, field profile plots have been generated. The field profiles are most conveniently generated on the basis of the known (skew and normal) multipoles, a_n and b_n, using the complex multipole expansion formalism given in equation (6).

$$B_y + iB_x = B_{ref} \sum_n \left(\frac{R}{R_{ref}}\right)^n \left[(b_n \cos n\phi - a_n \sin n\phi) + i(b_n \sin n\phi + a_n \cos n\phi)\right] \qquad (6)$$
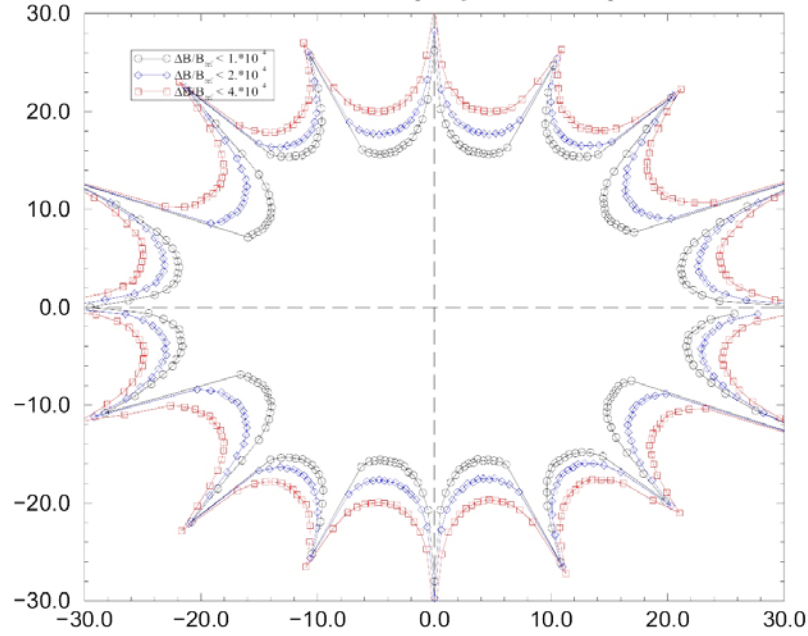
Figure 18: "Good-Field Region" plot for Tevatron dipoles. The contours of $<10^{-4}$, $<2 \cdot 10^{-4}$, $<4 \cdot 10^{-4}$, field variation (with respect to the 2D cross-sectional dipole field) have been calculated for the body-end combined, measured geometric (up-down average at 2000 A) multipole distribution averaged over all Tevatron dipoles installed (such as reported in Table 1). Distances from the bore center are in mm.
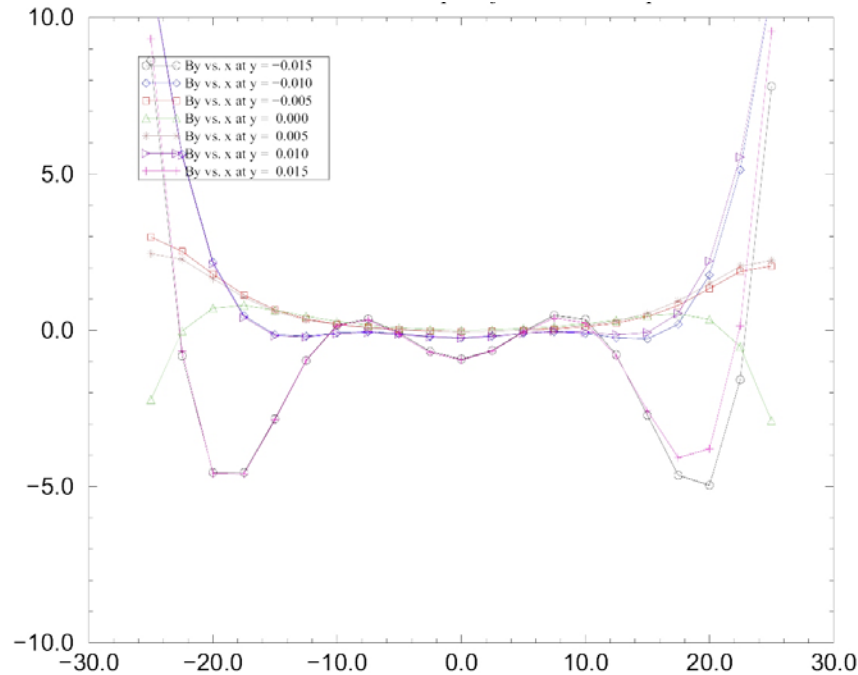

Figure 19: Cross-sectional Tevatron dipole profiles of the vertical magnetic field variation $\Delta B_y(x)/B_y(x)$ in units of 10^{-4}. The parameter of the different plots is the vertical distance y from the center. The fields were calculated for the body-end combined, measured geometric (up-down average at 2000 A) multipole distribution averaged over all Tevatron dipoles installed (such as reported in Table 1). Distances from the bore center are in mm.

A particular field profile plot, such as shown in Figure 18, plots the boundary of the region in which the field variation is less than 1-4 units of 10^{-4} of the main cross-sectional dipole field. Such plots give a good visual impression of the boundaries of the high field quality region. Most obvious in Figure 18 is the elliptical shape of the "good-field" region, which was deliberately chosen for the Tevatron because of initial assignment as a fixed target machine.

Another field plot with high educational value contains cross-sectional field profiles such as shown in Figure 19.

6)　Magnetization and Hysteresis Loops

The magnetic field models discussed above describe the geometric field properties and do therefore not include the effect of superconductor magnetization. The magnetization contribution essentially produces a small, current-dependent deviation from the geometric field components, giving rise to a hysteretic behavior. The following presents calculations of the hysteretic loops due to the superconductor magnetization obtained with the Roxie9.0 code. In particular the magnetization loops for the main field B_0 and for the major allowed multipoles b_2 and b_4 have been computed and are shown below together with experimental data.

The most important input parameter for the calculation of the magnetization effect is the critical current density, J_c, of the superconductor material. The program calculates the magnetization response of the superconducting strands directly from the critical current density and the strand and cable geometry parameters as well as the coil cross-section discussed in chapter 3.2. Note that the calculations discussed apply only to the magnetization contribution in the body of the Tevatron dipoles.

The following parametrization of the J_c of NbTi as a function of operating temperature and magnetic field from L. Bottura [4], combined with Lubell's laws [5], has been found to fit best the experimental strand critical current data.

$$T_c(B) = T_{c0}\left(1 - \frac{B}{B_{c20}}\right)^{\frac{1}{n}}$$
(7a)

$$B_{c2}(T) = B_{c20}\left[1 - \left(\frac{T}{T_{c0}}\right)^{n}\right]$$
(7b)

---

[4] "A Practical Fit for the Critical Surface of NbTi", L. Bottura, IEEE Trans. On Applied Superconductivity, Vol. 10, No. 1, March 2000
[5] "Empirical Scaling Formulas for Critical Current and Critical Field for Commercial NbTi", M.S. Lubell, IEEE Transactions on Magnetics 19, p. 754, 1983

$$j_c\left(B,T\right)= j_{cREF}\left(5T,4.22K\right)\frac{C_0}{B}\left[\frac{B}{B_{c2}(T)}\right]^\alpha\left[1-\frac{B}{B_{c2}(T)}\right]^\beta\left[1-\left(\frac{T}{T_{c0}}\right)^n\right]^\gamma \qquad (7c)$$

Typical constants for LHC strands, which were also applicable to the Tevatron strand material are given in Table 15.

Table 15: Parameters for the fit of the critical surface of NbTi.

T_{c0}	B_{c20}	n	C_0	α	β	γ
9.5 K	14.5 T	1.7	27.6	0.63	1	2.3

The reference current density j_{cREF}(4.22K,5T) is usually calculated from a measured critical current using the above relation "in reverse". J_{cREF}(4.22K,5T) is typically 3000 A/mm^2 for SSC and LHC type strands. Although Tevatron strands from the late production stages ("hiho-material") achieved 1800 A/mm^2, [7], 1500 A/mm^2 was chosen in the calculation presented below because it produces the experimentally observed b2 loop width. Also note that the critical current density is normalized on the non-Copper area in the strand cross-section.

The Tevatron magnet strand and cable geometry implemented in the models is summarized in Table 16.

Table 16: Parameters of the cables/strands of the Tevatron dipole magnets.

N strands	strand $\varnothing$	Cu/NCu ratio	filament $\varnothing$	N filaments/strand	Jc (5T, 4.22 K)
23	0.68 mm	1.7	9 μm	2114	1500 A/mm^2

Error! Reference source not found., Figure 20 and Figure 21 show a comparison of measured and calculated b_0, b_2 and b_4 magnetization loop data. Calculations were not only performed with Roxie but also with another, independent program, Maelstrom[6]. The measurements were performed with rotating coils in the body of Tevatron dipole TC 1220. Note that the geometric multipoles have been removed and the loops are therefore centered on zero. Also note that b_0 refers to the usual units of 10^{-4} of the main dipole field. Measurements and calculations were performed at 4 K. The good agreement between experimental and model data indicates that the hysteretic behavior of the Tevatron dipole magnets is well understood.

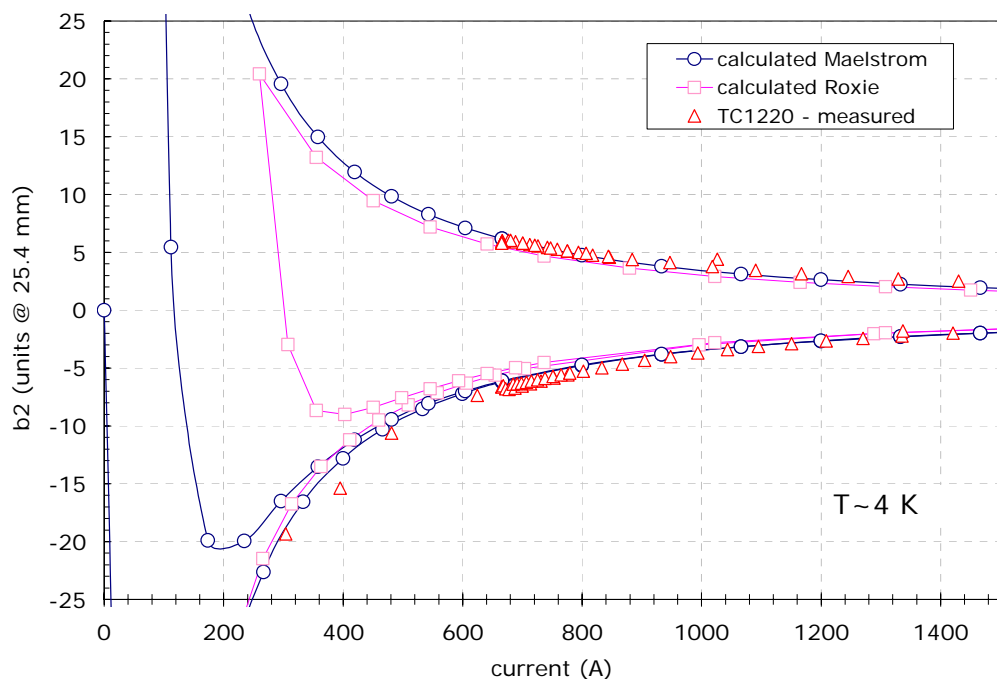[6] L. Bottura / CERN, personal communication, February 2004.

Figure 20: Comparison of calculated and measured b_2 magnetization loop in Tevatron dipole.
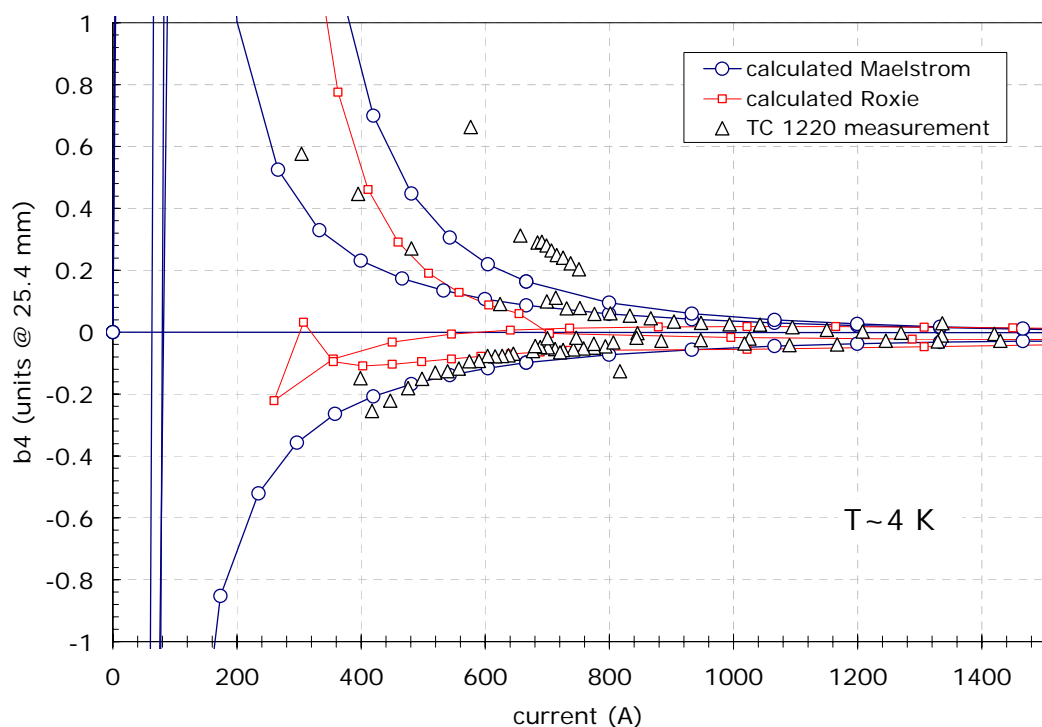

Figure 21: Comparison of calculated and measured b_4 magnetization loop in Tevatron dipole. Note that a slope (~-0.2 units / 1500 A) was removed from the measured b4 loop. The origin of this slope, which was also found in the original measurements in 1980, is not yet understood.

7)   References

1   R. Hanft et al., "Magnetic Field Properties of Fermilab Energy Saver Dipoles", TM-1182, 1630, 03/1983
2   N. Gelfand, personal communication;
3   Fermilab Magnet Test Facility measurements, 1980-1993, R. Hanft, editor, unpublished
4   L. Lederman et al., "Design Report 1979, Superconducting Accelerator"
5   A. Devred, "1999 Review of Superconducting Dipole and Quadrupole Magnets for Particle Accelerators", CEA/DAPNIA/STCM 99-24, Dec. 1999
6   R. Hanft et al., "Studies of time dependence of fields in Tevatron superconducting dipole magnets", IEEE Transactions on Magnetics, Vol. 25/No 2/ p. 1647, March 1989
7   M.A. Green, "Calculating the Jc(B,T) Surface for Niobium Titanium using a Reduced-State Model", IEEE Transactions on Magnetics, Vol. 25, N.2, March 1989